Modeling of Pressure and Temperature Profiles for the Flow of CO_2 through a Restriction

A Leyli[1]*, S Jackson[1], H Khawaja[1,2], M Moatamedi[2,3]

1. UiT – The Arctic University of Norway
2. Al Ghurair University, UAE
3. Oslo Metropolitan University, Norway

ABSTRACT

CO_2 emissions due to massive industrialization have led to several environmental issues. Carbon Capture and Storage (CCS) is one of the most important technologies that can be used to reduce anthropogenic CO_2 emissions worldwide. CCS projects mainly involve three processes: carbon capture, transportation, and storage. In the transportation process, the modeling of the flow in pipelines and the relationships between pressure, flow velocity, temperature, density, and phase stability are of significance. Orifice plates are a common tool used for flowrate measurements. Several standards provide the specifications and implementation approach for this type of equipment item in pipelines. In this study, flow through an orifice plate is simulated with computational fluid dynamics (CFD) modeling software, namely ANSYS®, to obtain fluid pressure, velocity, and temperature profiles. Model geometry and fluid properties are defined that are suitable for making a comparison with ISO-5167 empirical correlations and a similar reference study, which are used to validate the simulation results. A mesh sensitivity analysis is conducted to ensure the correctness of the results. A reasonable agreement is found between the simulation results, empirical correlations, and previous studies. The Joule_Thompson cooling effect is also studied in this work for high-pressure CO_2 cases, and the results show good agreement with reference studies.

1. INTRODUCTION

The rapid increase of industrialization has led to massive CO_2 production globally, which consequently brings up environmental and climate issues [1]. Fossil fuels will continue to be the primary source of energy in the near future [2]. Carbon Capture and Storage (CCS) is an important technology that allows the reduction of anthropogenic CO_2 emissions. CCS projects in general consist of three different processes: CO_2 capture, transportation, and storage. For CO_2 transportation, modeling of the flow in pipeline systems, including the relationships between pressure, density, flow velocity, phase stability, and temperature, is necessary [3-9].

Orifice plates are a common type of device used for flow measurement in industries due to their ease of use and reliability. Circular, rectangular, and square orifice shapes are all available, each type has its advantages and disadvantages [10-12]. Various parameters affect the flow through orifice plates. For example, a critical element for the prediction of

*Corresponding Author: amir.n.leyli@uit.no

square-edged orifice plates discharge coefficient is the precise shape of the edge. A small change in the orifice diameter can also alter the discharge coefficient considerably [13, 14].

Several standards, including ISO-5167 and BS-1042, provide related information for these devices. ISO-5167 includes four-parts in which it covers specification, implementation approach, and error calculations for orifice plates, nozzles, and venturi tubes installed in pipelines to measure flowrate. ISO-5167 can only be applied to pressure differential devices for subsonic flow velocities, single-phase and non-pulsating flows within a limited range of pipe size and Reynolds number. Part two of ISO-5167 specifies orifice plates with different pressure tapings [15]. The BS-1042 standard is technically equivalent to ISO-5167, but has some minor modifications, text clarifications, and British measurement units [16].

Wherever there is a restriction in a pipeline, the fluid velocity inside the pipeline increases, thus making a low-pressure area downstream of the restriction. The pressure reduction is proportional to the flowrate; therefore, it can be used to calculate the flowrate indirectly. The arrangement related to this type of flowmeter is shown in Figure 1 [17].

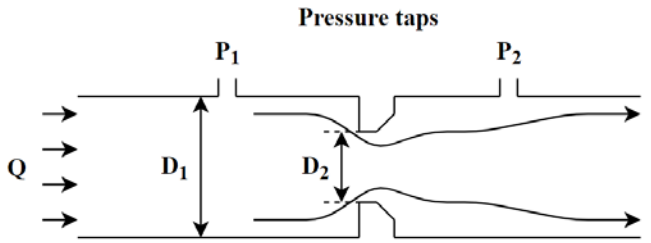

Figure 1 - Orifice plate arrangement in a pipeline

The design of this type of flow measuring device is developed by certain standardized empirical correlations. These correlations are used to verify the model simulated by CFD methodology with ANSYS® software in this work. CFD is the most common methodology which uses numerical analysis to simulate fluid behavior [18-22]. In general, the basis for CFD analysis is three fundamental physical principles, including conservation of mass, momentum, and energy. These principles are defined by Navier Stokes equations as shown in Equations (1-5) [9, 23-25].

$$\frac{\partial \rho}{\partial t} + \frac{\partial(\rho u)}{\partial x} + \frac{\partial(\rho v)}{\partial y} + \frac{\partial(\rho w)}{\partial z} = 0 \quad (1)$$

$$\rho \frac{du}{dt} = -\frac{\partial p}{\partial x} + \frac{\partial \tau_{xx}}{\partial x} + \frac{\partial \tau_{yx}}{\partial y} + \frac{\partial \tau_{zx}}{\partial z} + \rho f_x \quad (2)$$

$$\rho \frac{dv}{dt} = -\frac{\partial p}{\partial y} + \frac{\partial \tau_{xy}}{\partial x} + \frac{\partial \tau_{yy}}{\partial y} + \frac{\partial \tau_{zy}}{\partial z} + \rho f_y \quad (3)$$

$$\rho \frac{dw}{dt} = -\frac{\partial p}{\partial z} + \frac{\partial \tau_{xz}}{\partial x} + \frac{\partial \tau_{yy}}{\partial y} + \frac{\partial \tau_{zz}}{\partial z} + \rho f_z \quad (4)$$

$$\frac{D}{Dt}\left(e+\frac{V^2}{2}\right)=\rho Q+\frac{\partial}{\partial x}\left(k\frac{\partial T}{\partial x}\right)+\frac{\partial}{\partial y}\left(k\frac{\partial T}{\partial y}\right)+\frac{\partial}{\partial z}\left(k\frac{\partial T}{\partial z}\right)-\frac{\partial(up)}{\partial x}-\frac{\partial(vp)}{\partial y}-\frac{\partial(wp)}{\partial z}+\frac{\partial(u\tau_{xx})}{\partial x}+\frac{\partial(u\tau_{yx})}{\partial y}+\frac{\partial(u\tau_{zx})}{\partial z}+\frac{\partial(v\tau_{xy})}{\partial x}+\frac{\partial(v\tau_{yy})}{\partial y}+\frac{\partial(v\tau_{zy})}{\partial z}+\frac{\partial(w\tau_{xz})}{\partial x}+\frac{\partial(w\tau_{yz})}{\partial y}+\frac{\partial(w\tau_{zz})}{\partial z}+\rho\vec{f}.\vec{V} \quad (5)$$

where ρ (kg/m^3) is the density, t (s) is time, x, y, and z are Cartesian coordinates, u, v, and w are velocity components in x, y, and z directions, f (N) is body force per unit mass acting on the fluid element on Cartesian coordinates, τ (N/m2) is the shear stress tensor, τ_{ij} denotes stress in the j-direction exerted on a plane perpendicular to the i-axis, p (pa) is pressure, T (K) is temperature, e (J) is the internal energy, k (W/m.K) is thermal conductivity, Q (W/m^3) is energy generation term, p (Pa) is pressure and V (m/s) is the velocity field which can be defined by Eq (6).

$$\vec{V}(x,y,z,t)=\vec{u}i+\vec{v}j+\vec{w}k \quad (6)$$

where $u=\frac{dx}{dt}$, $v=\frac{dy}{dt}$, $w=\frac{dz}{dt}$. Navier_Stokes equations can take several different forms based on the problem. However, since they are partial differential equations (PDEs), they need to be solved numerically commonly in most cases [26-28].

The pressure drop in pipelines through a restriction is usually accompanied by a temperature drop for most fluids referred to as Joule_Thompson (JT) cooling. The extent of this temperature drop depends on the amount of pressure drop, the inlet pressure, temperature, and fluid properties. The precise modeling of the JT cooling is critical in high-pressure CO_2 systems where sudden cooling can cause phase change and possible freezing [1, 29-33].

2. METHODOLOGY

In this work, flow through an orifice plate in a pipeline is simulated with ANSYS®. The simulation model is compared with a selected model from the second part of the ISO 5167 standard. The simulated model is also validated against empirical correlations of ISO 5167 and a reference study by Prasanna and Seshdari [17].

2.1. Model development

Initially, the geometry of the orifice plate was developed as a 2-D asymmetric model according to ISO-5167 requirement for 15 diameters upstream distance and 25 diameters downstream distance. The model is symmetrized in a longitudinal direction in order to decrease the calculations. The selected upstream diameter, $D_1 = 80$ mm and the orifice diameter, $D_2 = 40$ mm, as illustrated in Figure 1, were specified to match the conditions in the reference study. The model 2-D configuration and specifications are shown in Figure 2 and Table 1 in turn.

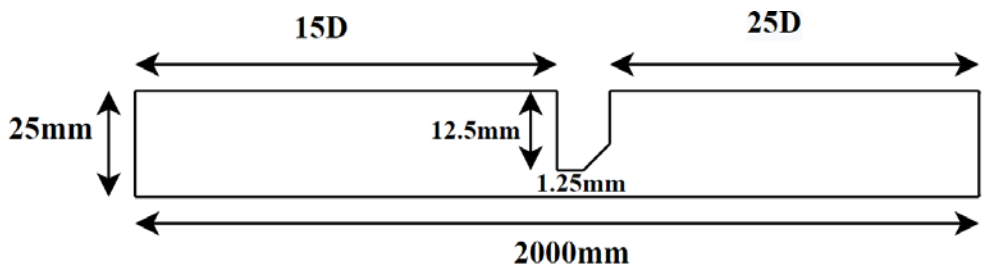

Figure 2 - 2-D model configuration

Table 1 - The model specifications

Variables	Values	Units
Diameter of pipe (D)	50	mm
Diameter of throat (d)	25	mm
Diameter ratio (β)	0.5	-
Upstream pipe length	15D	mm
Downstream pipe length	25D	mm
Thickness of the plate	3	mm
Type of OP beveled	45	degrees
1 mm straight hole followed by 45º beveling		

The geometry of the model was meshed by applying edge sizing alongside the pipe wall with 1000 divisions, which generates 22000 elements. A mesh sensitivity analysis was conducted to improve the accuracy of the results. The mesh configuration near the orifice is shown in figure 3.

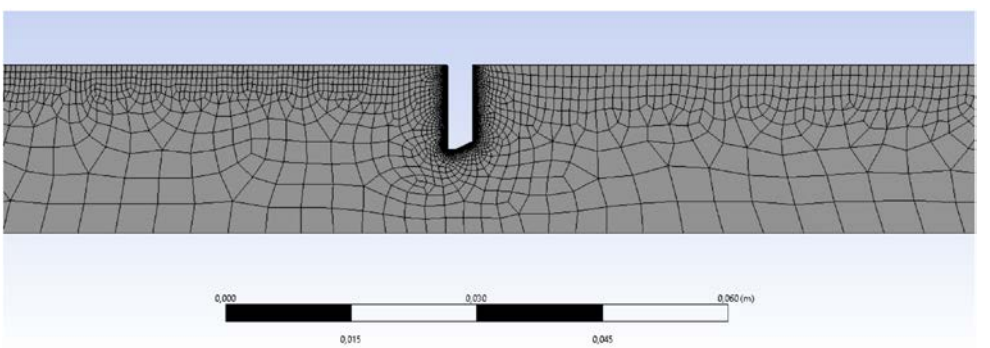

Figure 3 - Simulation model mesh configuration

To give a good comparison between the simulation and the reference study, all the boundary conditions and fluid properties were chosen as similar to the reference study. The fluid chosen was the air with a constant density of 1.225 kg/m^3. Symmetry was chosen for the axis in the longitudinal direction, velocity input for the inlet, pressure for the outlet (1 atm), no-slip for the walls, and the Spalart Allmars turbulence model were specified as the boundary conditions for the simulation approach.

2.2. Validation Study

The simulation model was validated in two ways: first, against the results of the reference study and second against the results of the empirical calculations set out in ISO-5167. The same model geometry and a constant Reynolds number of 105 were used for both cases, thus fixing an inlet velocity of 36.75 m/s. Using this inlet velocity, the results of the reference study were compared to the results of the simulation using $\Delta P/P$, where $\Delta P = P_1 - P_2$, P_1 is the upstream pressure and P_2 is the downstream pressure (See Figure 1).

According to correlations in ISO 5167, the mass flow rate of Q_m can be predicted by equation (1) given as:

$$Q_m = \frac{eC_d}{\sqrt{1-\beta^4}} \frac{\pi {D_2}^2}{4} \sqrt{2(P_1 - P_2)\rho_1} \tag{1}$$

where ρ_1 (kg/m^3) is the density of the fluid, C_d is the discharge coefficient of the orifice and e is the expansion coefficient. The values of C_d and e can be calculated given by Equations [2 & 3].

$$C_d = 0.5961 + 0.0261\beta^2 - 0.216\beta^8 + 0.00521\left(\frac{10^8\beta}{Re_D}\right)^{0,7} + (0.0188 + 0.0063A)\beta^{3,5}\left(\frac{10^6}{Re_D}\right)^{0,3} + (0.043 + 0.08e^{-10l_1} - 0.123e^{-7l_1})(1 - 0{,}11A)\frac{\beta^4}{1-\beta^4} - 0.031(M - 0.8M^{1,1})\beta^{1,3} + 0.011(0.75 - \beta)\left(2.8 - \frac{D}{25.4}\right) \tag{2}$$

$$e = 1 - (0.351 + 0.256\beta^4 + 0.93\beta^8)\left(1 - \left(\frac{P_2}{P_1}\right)^{\frac{1}{k}}\right) \tag{3}$$

where A = (1900. β / Re_D)^{0,8}, M = 2l_2/(1- β), $l_1 = L_1/D_1$, $l_2 = L_2/D_2$, L_1 (m) is the distance to the upstream tapping and L_2 (m) is the distance to the downstream tapping.

An analytical prediction of the value of ΔP is made through Equations 1 to 3 with two different fluid velocities. The results from empirical calculations can be seen in Table 2.

Table 2 - The analytical calculations

Variables	Values (u_1)	Values (u_2)	Units
D_1	0.05	0.04	m
D_2	0.025	0.020	m
u	30	36.75	m/s
μ	0.018	0.018	Pa.s
ρ	1.225	1.225	kg/m^3
Re	102083	100042	-
β	0.5	0.5	-
A	0.15	0.152	m^2
C_d	0.610	0.610	
Q_m	0.0722	0.0566	kg/s
$P_1 - P_2$	22202	33310	Pa
k	1.4	1.4	
e	0.947	0.923	
$P_1 - P_2/e$	23457	36097	Pa

2.3. Model Optimization

Based on the validation results, it was recognized that the ISO requirements of 15 diameters upstream and 25 diameters downstream are not required in the model to calculate an accurate pressure and velocity profile across the orifice plate. Thus, to reduce the calculation time, the upstream and downstream lengths were reduced in a stepwise trial and error process that ensured that the accuracy of the results was not significantly reduced.

Once the optimum horizontal extent of the model had been decided, the mesh size was studied to determine if fewer elements would provide sufficient calculation accuracy and stability. Therefore, the mesh edge sizing was changed from 1000 number of divisions to 500, 250, and 100. The pressure profile along the longitudinal axis was used as an indication of mesh quality.

2.4. High-Pressure Flow of CO_2

In this work the flow of high-pressure CO_2 in the pipeline restricted by orifice plate is studied. A set of studies is conducted which has investigated the effect of the property calculation approach on pressure and temperature profiles for both air and CO_2 as the operating fluids. Finally, the results of the Joule_Thompson (JT) effect are compared with the work of the reference study [1].

3. Results and Discussion

Results are provided in two sections: first, a short summary of the validation and model optimization results is presented; second, a brief summary of the results for the modeling of high-pressure CO_2 flow is presented.

3.1. Validation and Model Optimization

The validity of the modeling method was partly determined by comparing the pressure profile along the wall of the simulation case with the calculated $\Delta P/P_1$. Furthermore, empirical calculations were performed to obtain the values of C_d and $\Delta P/P_1$. Figure 5 shows the pressure profile alongside the wall of the pipeline, and Table 3 contains the details of the empirical calculations.

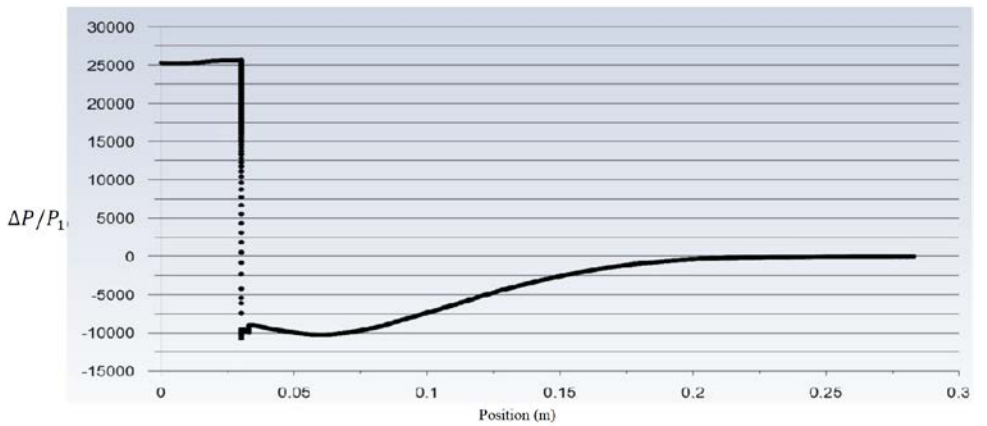

Figure 4 - Pressure Profile in Pascal along the wall for the validation case illustrating $\Delta P/P_1$

Table 3 - Summary of validation results

	CFD (ANSYS® Fluent)	**ISO Standard**
C_d	0.6103	0.6058
$\Delta P/P_1$	0.2800	0.2571
ΔP (Pa)	35000	36100

The generated results from the Figure 5 plot are presented in table 3, along with the comparison of the results of the simulation and reference study. It is to be noted that in the reference study the C_d equivalent calculated by the model is back calculated.

Table 3 shows that according to the reference article, the ISO value of C_d should be 0.6058 when $Re = 10^5$, and according to the empirical calculations, the has the value of 0.6103. This represents a good agreement (less than 1% error) between the two independent sets of calculations. The ΔP calculated is then 36 100 (Pa), which compares well with that calculation in the simulation. The validation results show reasonable agreement between $\Delta P/P_1$ value between the reference study and the simulation.

After validating the model against the empirical correlations, several attempts are made to investigate if the length (size) of the model could be reduced whilst maintaining the accuracy of the results. Figure 6 shows how the velocity in the profile varies over the region around the orifice.

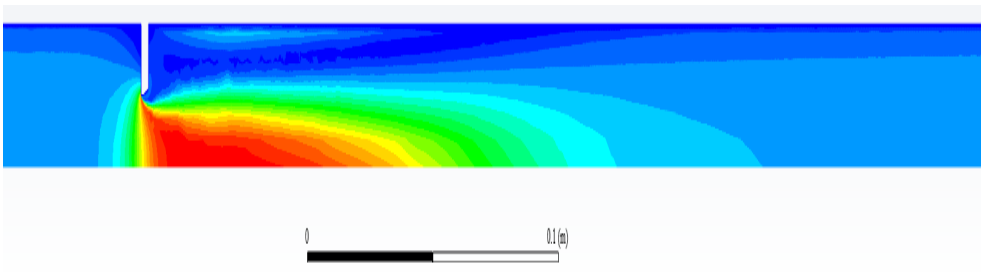

Figure 5 - Velocity contour around the orifice

Based on the profiles shown in figure 6, a new model with an upstream distance of 30 mm and a downstream distance of 250 mm was constructed and tested for accuracy using the pressure profile along the wall to compare against the validation case.

In this smaller model, a mesh edge sizing of 500 divisions was used to ensure that the resolution in the model was equal or better than that of the validation case. Figure 7 shows the pressure profile for the reduced length model and illustrates reasonable agreement compared to Figure 5.

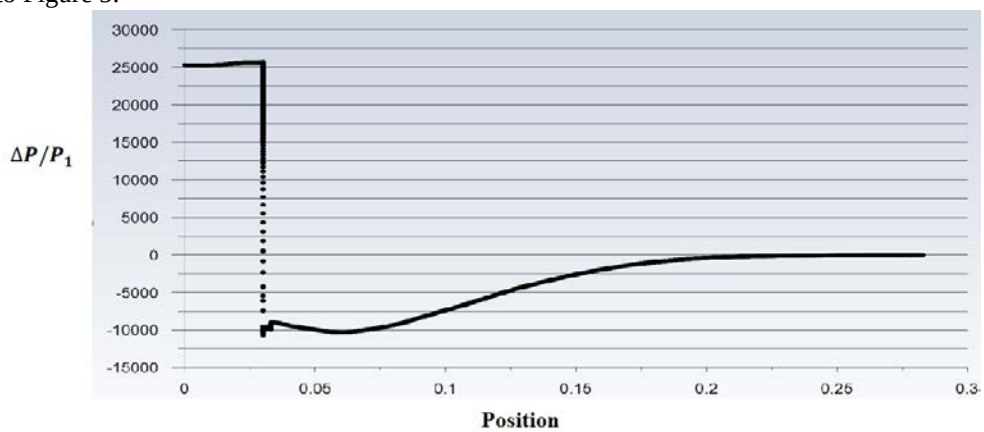

Figure 1 - Pressure Profile in Pascal along the wall for the Reduced Length (RL) case illustrating $\Delta P/P_1$

Since the reduced length model had been shown to be accurate, a study was conducted to investigate if a reduction in the mesh density could be made whilst maintaining accuracy; thus, mesh edge sizing was changed from 500 to 250 and 100 number of divisions.

The velocity profile for different mesh sizing is presented in Figure 8. Although the results show that the edge sizing with 250 and 100 number divisions maintains most of the features of the 500-element edge sizing, later simulation runs showed that this model was unstable in some cases and, therefore, the 500-element edge sizing is used in all of the subsequent modeling work.

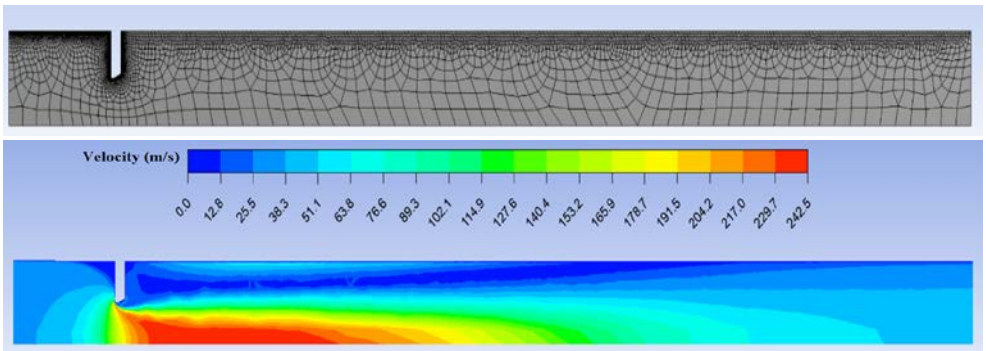

(a)

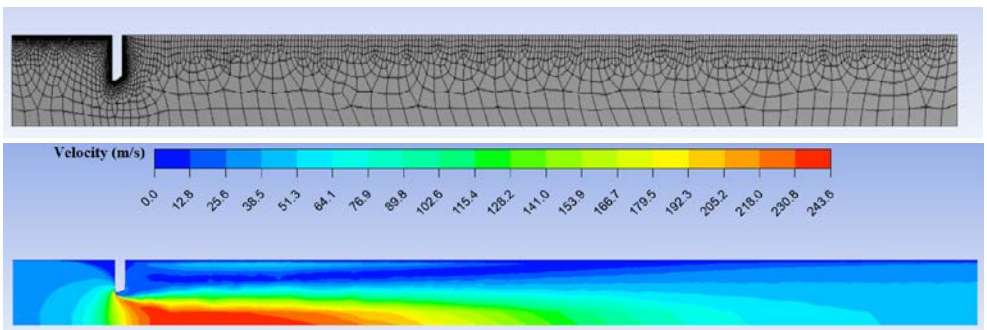

(b)

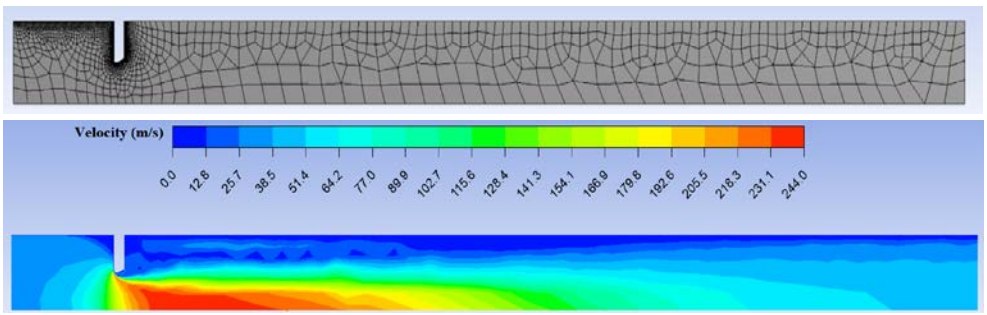

(c)

Figure 7 - Mesh sensitivity analysis and velocity contours for (a) 500 (b) 250 and (c) 100 number of edge sizing

3.2. Results for the Compressible Flow of Air

Once the model size and mesh size had been optimized, the impact of the fluid properties model was investigated. In the previous part of the analysis and the reference study, a constant density for air had been used. In Figures 9 and 10, the impact of specifying an Ideal Gas (IG) model for density and using the Peng Robinson (PR) equation of state (EOS) model are presented.

The results presented in Figures 9 and 10 were generated using an inlet velocity of 36 m/s, corresponding to a maximum Mach of 0.9. They illustrate significantly different pressure and velocity profiles compared to the compressible flow of air, implying that the constant density assumption used in the reference study and the validation work is not sufficiently accurate to model the pressure profile through the orifice. Both the IG and PR models show that the maximum velocity is around 20 m/s higher than the constant density model, and the pressure drop is around double that calculated in the earlier work, which is reasonable given that $\Delta P \propto v^2$ according to Bernoulli's equation.

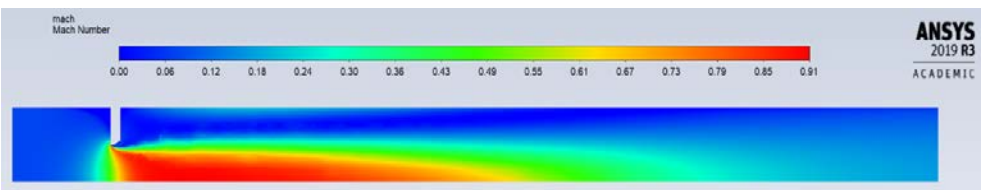

(a)

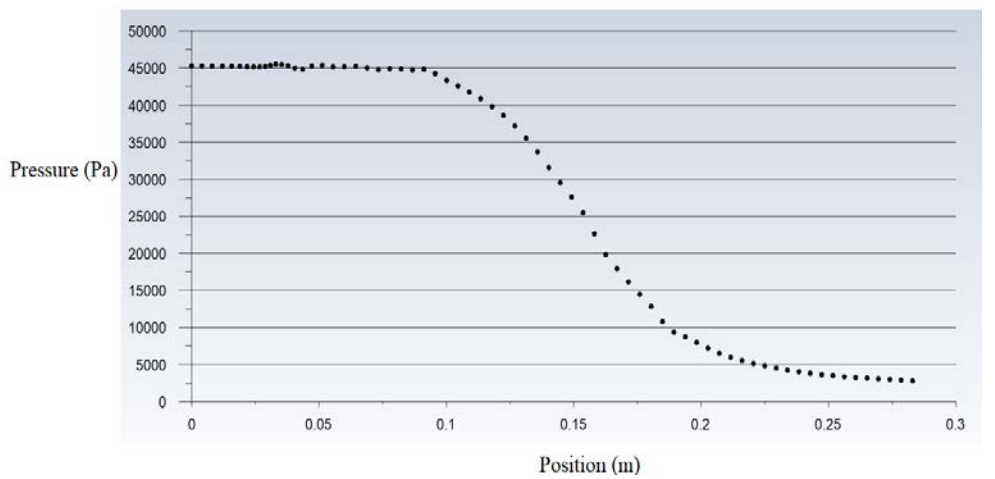

(b)

Figure 8. Air with Ideal Gas EOS and 0 MPa outlet pressure (a) Mach No. contour (b) pressure profile

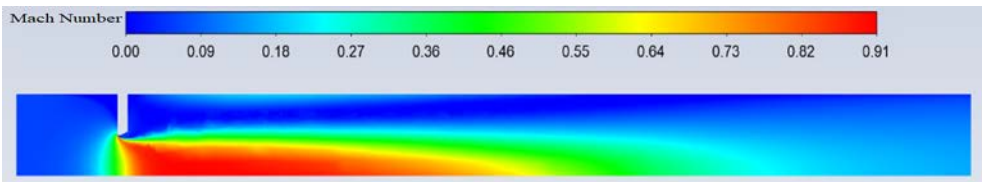

(a)

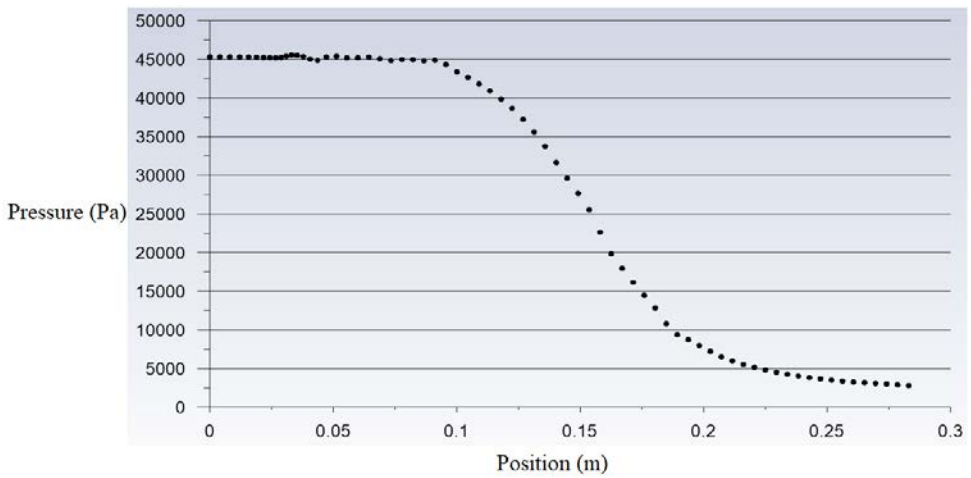

(b)

Figure 9 - Air with PR EOS and 0 MPa outlet pressure (a) Mach No. (b) Pressure Along the Axis

Although these results highlight inaccuracy in the constant density assumption used in earlier modeling work, they do agree very closely with each other, giving confidence in the accuracy of the compressible flow modeling basis.

3.3. The compressible flow of CO_2 and Joule_Thompson (JT) Cooling

The modeling of CO_2 was conducted on the basis of the results obtained for the compressible flow of air at low pressure. Initially, runs were made at low pressure and subsequently at 0.5 and 2.0 MPa gauge pressures. Because CO_2 has a substantially higher molecular weight compared to air and consequently a lower sonic velocity, the inlet velocity was reduced to avoid supersonic flow. All of the results presented in this section are correlated against the Mach number rather than velocity.

Figure 11 shows the temperature profile for a constant Mach number in different operating gauge pressures. The JT cooling effect can be seen through the profile. The results show that more cooling occurs at higher pressure, where the absolute value of the pressure drop is higher given the same Mach number compared to lower pressure cases. The results also show that there is substantial variation in temperature across the diameter of the pipe downstream of the orifice.

The results also show that there is substantial variation in temperature across the diameter of the pipe downstream of the orifice.

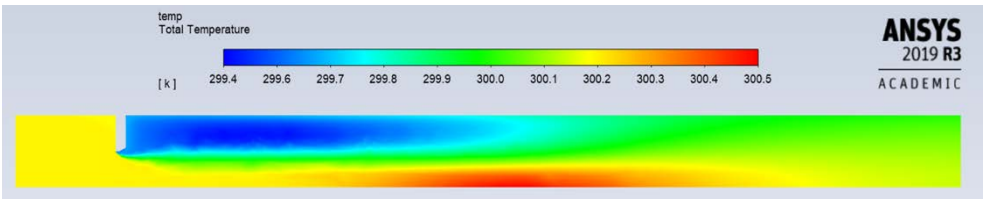

(a)

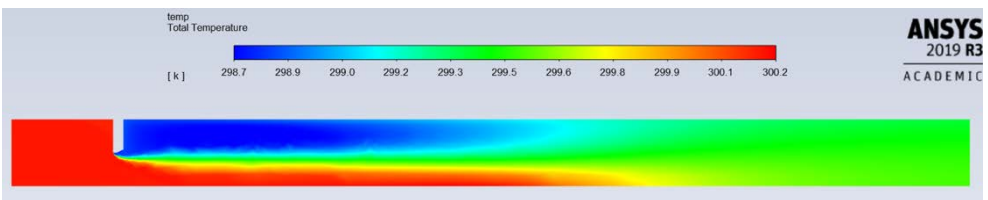

(b)

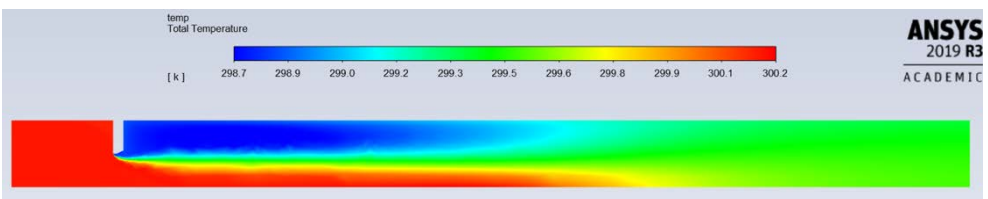

(c)

Figure 10. Impact of Pressure on Temperature at constant Mach = 0.5 & Pressure = (a) 0 MPa (g) (b) 0.5 MPa (g) (c) 2 MPa (g)

Figure 12 presents the pressure and temperature plot for 2 MPa operating gauge pressure and Mach No. equal to 0.8 alongside the wall and symmetry axis for CO_2 as operating fluid and using PR model as EOS. In Figure 12 (a) the instant pressure drop through the restriction can be seen. The pressure drop occurs with quietly same trend alongside the symmetry axis and the wall. Figure 12 (b) shows the temperature plot against the pipeline length for the symmetry axis and the wall. The temperature drop and JT cooling effect can be seen in through an instant reduction in the temperature value by CO_2 flow passage through the orifice. In addition, the plots represent a JT coefficient curve of 10.8 K per MPa, which correlates well with the data presented by the reference study for 300 K and 2 MPa gauge pressure operating conditions.

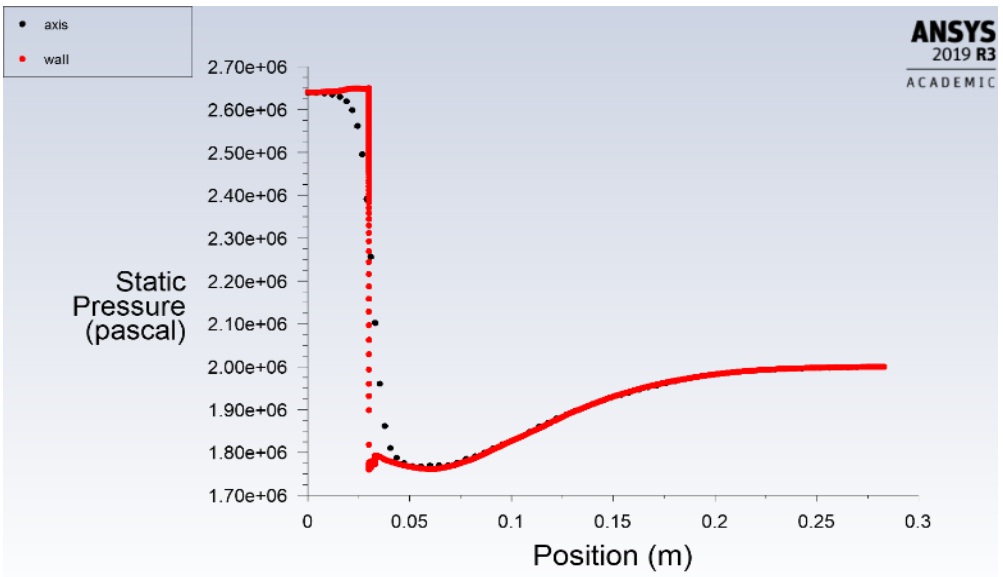

(a)

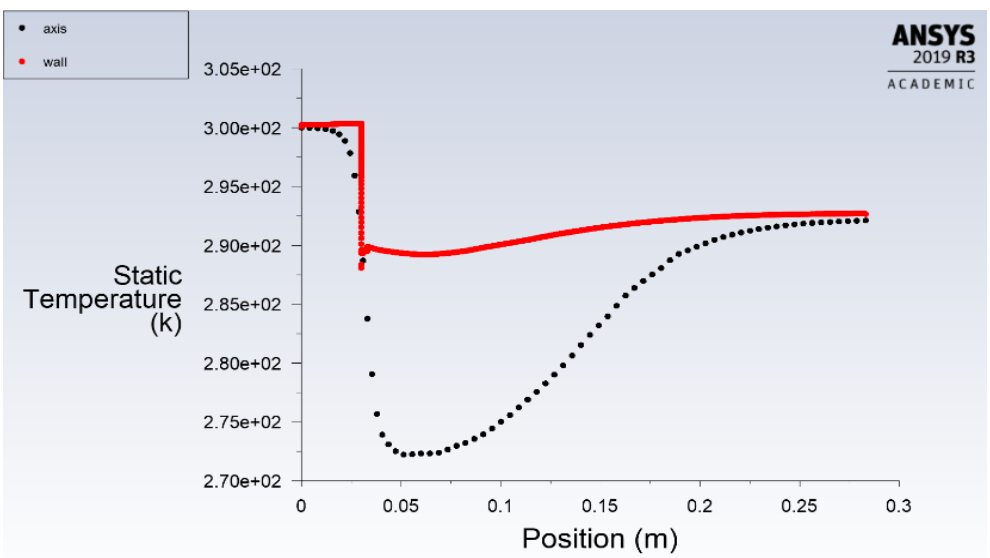

(b)

Figure 12. CO_2 with PR as the EOS, JT Effect at 2 MPa(g) and Mach = 0.8 (a) Pressure in MPa(g) along the wall and axis (b) temperature along the wall and axis.

4. CONCLUSION

Within this work, a model for the flow through an orifice has been developed and optimized. The results of the model are verified against previous study work for incompressible flow, showing reasonable agreement with both empirical calculations and other published results. Application of the verified modeling approach for incompressible flow to compressible flow cases using both the IG equation and PR for density calculations revealed significant differences in the predictions for incompressible and compressible flow. However, a good agreement between the results for the IG and PR modeling basis indicates that the inaccuracy lies in the simplified compressible flow assumption used in the first part of the modelling work. This does not mean that the approach used in the verification work is fundamentally flawed, but rather that for the value of $\Delta P/P_1$ found in the verification work, the compressible flow assumption is not accurate.

Using the PR EOS as the basis for property calculations and CO_2 as the working fluid, further study was made for the temperature profile to associate with flow across the orifice. The results for the JT coefficient were correlated with other study work for cases where the outlet pressure was 2 MPa(g) and the inlet temperature of 300 K. The results showed good agreement between simulation results and reference study, providing a new validation of the modeling basis.

ACKNOWLEDGMENT

The publication charges for this article were funded by a grant from the publication fund of UiT-The Arctic University of Norway.

REFERENCES

[1] Wang, J., Z. Wang, and B. Sun, Improved equation of CO2 Joule–Thomson coefficient. Journal of CO2 Utilization, 2017. 19: p. 296-307.

[2] Jackson, S., O. Eiksund, and E. Brodal, Impact of Ambient Temperature on LNG Liquefaction Process Performance: Energy Efficiency and CO2 Emissions in Cold Climates. Industrial and Engineering Chemistry Research, 2017. 56(12): p. 3388-3398.

[3] Jackson, S. and E. Brodal. A comparison of the energy consumption for CO2 compression process alternatives. in IOP Conference Series: Earth and Environmental Science. 2018.

[4] Jackson, S., Development of a model for the estimation of the energy consumption associated with the transportation of CO2 in pipelines. Energies, 2020. 13(10).

[5] Brodal, E., S. Jackson, and O. Eiksund, Energy Saving Potential of CO2 Transportation Processes in Cold Climate Locations. Industrial and Engineering Chemistry Research, 2016. 55(44): p. 11597-11605.

[6] Jackson, S. and E. Brodal, Optimization of the CO2 liquefaction process-performance study with varying ambient temperature. Applied Sciences (Switzerland), 2019. 9(20).

[7] Jackson, S. and E. Brodal, Optimization of the energy consumption of a carbon capture and sequestration related carbon dioxide compression processes. Energies, 2019. 12(9).

[8] Brodal, E., S. Jackson, and O. Eiksund, Transient model of an RSW system with CO2 refrigeration – A study of overall performance. International Journal of Refrigeration, 2018. 86: p. 344-355.

[9] Khawaja, H.A., Sound waves in fluidized bed using CFD–DEM simulations. Particuology, 2018. 38: p. 126-133.

[10] Mehmood, M.A., et al., CFD study of pressure loss characteristics of multi-holed orifice plates using central composite design. Flow Measurement and Instrumentation, 2019. 70.

[11] Morrison, G.L., et al., Comparison of orifice and slotted plate flowmeters. Flow Measurement and Instrumentation, 1994. 5(2): p. 71-77.

[12] Thurston, G.B., Nonlinear Acoustic Properties of Orifices of Varied Shapes and Edge Conditions. Journal of the Acoustical Society of America, 1958. 30(5): p. 452-455.

[13] Brain, T.J.S. and J. Reid, MEASUREMENT OF ORIFICE PLATE EDGE SHARPNESS. Measurement and Control, 1973. 6(9): p. 377-383.

[14] Mishra, D.P. and D. Mishra, Augmentation of local and average heat transfer to an impinging air jet using orifice. International Journal of Turbo and Jet Engines, 2005. 22(4): p. 225-235.

[15] ISO-5167, Measurement of fluid flow by means of pressure differential devices inserted in circular-cross section conduits running full, in Orifice Plates. 2003: Switzerland.

[16] BSI-1042, Measurment of Fluid flow in closed conduits. 1981.

[17] Prasanna, M., V. Seshadri, and Y.K. KJ, Analysis of Compressible Effect in the Flow Metering By Orifice Plate Using CFD. International journal of scientific research in science engineering and technology (IJSRSET). ISSN, 2016: p. 2395-1990.

[18] Khawaja, H. and M. Moatamedi, 2 - Methodology: computational fluid dynamics-discrete element modeling of fluidized beds, in Multiphysics Modelling of Fluid-Particulate Systems, H. Khawaja and M. Moatamedi, Editors. 2020, Academic Press. p. 23-49.

[19] Khawaja, H.A. and M. Moatamedi, 1 - Introduction: discrete element modeling-computational fluid dynamics of fluidized beds, in Multiphysics Modelling of Fluid-Particulate Systems, H. Khawaja and M. Moatamedi, Editors. 2020, Academic Press. p. 3-22.

[20] Khawaja, H. and M. Moatamedi, 3 - Validation case study: bubbling in the fluidized bed, in Multiphysics Modelling of Fluid-Particulate Systems, H. Khawaja and M. Moatamedi, Editors. 2020, Academic Press. p. 51-74.

[21] Myrvang, T. and H. Khawaja, Validation of air ventilation in tunnels, using experiments and computational fluid dynamics. The International Journal of Multiphysics, 2018. 12(3): p. 295-312.

[22] Brunner, D., et al., CFD modelling of pressure and shear rate in torsionally vibrating structures using ANSYS CFX and COMSOL Multiphysics. The International Journal of Multiphysics, 2018. 12(4): p. 349-358.

[23] Leyli, A., et al., Multiphysics Study of Forced Convection Conjugate Heat Transfer (CHT) Problem. The International Journal of Multiphysics, 2019. 13(3): p. 215-230.

[24] Leyli, A., et al., Conjugate Heat Transfer Model Based on SIMPLE and Coupled Energy and Heat Equations. The International Journal of Multiphysics, 2020.

[25] Khawaja, H., et al., Fluid solid interaction simulation of CFRP shell structure. Mathematics in Engineering, Science and Aerospace MESA, 2017. 8: p. 311-324.

[26] Khawaja, H. and M. Moatamedi, Semi-Implicit Method for Pressure-Linked Equations (SIMPLE) – solution in MATLAB®. The International Journal of Multiphysics, 2018. 12(4): p. 313-326.

[27] Nordli, A. and H. Khawaja, Comparison of Explicit Method of Solution for CFD Euler Problems using MATLAB® and FORTRAN 77. The International Journal of Multiphysics, 2019. 13(2): p. 203-214.

[28] Brunner, D., et al., Analysis of a Tubular Torsionally Resonating Viscosity–Density Sensor. Sensors, 2020. 20(11): p. 3036.
[29] Gross, S., Infrared sensor cooling by the Joule-Thompson effect. Infrared Physics, 1966. 6(2): p. 47-56.
[30] Ladokhin, S.D., A.I. Lunin, and Y.N. Subbotin, Investigation of the Joule-Thompson cycle using mixtures at liquid-nitrogen temperatures. Chemical and Petroleum Engineering, 1992. 28(9): p. 547-551.
[31] Grossman, E., E.M. Glauser, and S.C. Glauser, Joule-Thompson coefficient for anesthetic gases. Anesthesiology, 1973. 38(3): p. 280-282.
[32] Bonne, F., et al. Nonlinear observer of the thermal loads applied on the helium bath of a cryogenic Joule-Thompson cycle observer design and experimental validation. in IFAC Proceedings Volumes (IFAC-PapersOnline). 2013.
[33] Rostami, M., et al., Charged accelerating AdS black hole of f (R) gravity and the Joule-Thomson expansion. International Journal of Geometric Methods in Modern Physics, 2020. 17(9).